48th AIAA/ASME/SAE/ASEE Joint Propulsion Conference & Exhibit
30 July - 01 August 2012, Atlanta, Georgia

AIAA 2012-3843

Magnetic Nozzle Far-Field Simulation

M. Merino* and E. Ahedo†
Universidad Politécnica de Madrid, Madrid 28040 Spain

An analysis of the far-field plasma plume generated by a magnetic nozzle is presented, covering (1) the residual forces on the plasma in the downstream region, (2) the ion self-detachment from the magnetic field and free-plume formation, and (3) a preliminary investigation of secondary physical mechanisms that affect the plasma jet. This study is based on an extended version of our DIMAGNO code that allows simulation beyond the magnetic nozzle turning point. Results for different magnetization degrees show that ions naturally detach from the magnetic field and that the bulk of the plasma does not turn back along the magnetic field, supporting the viability of these devices for plasma propulsion.

Downloaded by Eduardo Ahedo on November 25, 2012 | http://arc.aiaa.org | DOI: 10.2514/6.2012-3843

I. Introduction

A magnetic nozzle (MN), consisting of an applied convergent-divergent axysimmetric magnetic field, constitutes the main acceleration stage of several advanced plasma propulsion concepts. Illustrative examples are the Helicon thruster,[1–4] the applied-field MPD thruster[5,6] and the Variable Specific Impulse Magnetoplasma rocket (VASIMIR).[7] The purpose of the MN is to harness and control the expansion of the hot plasma in order to deliver a high-velocity, efficient plasma beam, while keeping plasma-wall contact to a minimum. The plasma acceleration through the nozzle results in a magnetic reaction force on the magnetic circuit of the device, producing thrust.[8] An additional possible advantage of MNs is their ability to tailor thrust and specific impulse in-flight to different mission requirements by changing the geometry and intensity of the applied field.

The plasma in a MN can be roughly divided into two zones: in the acceleration region (or near-field), the supersonic plasma expansion is dominated by the interplay between pressure and magnetic forces. The largest fraction of thrust is generated here. In the detachment region (or far-field), most of the internal energy of the plasma has been already converted into directed kinetic energy, and its evolution is subject to the residual pressure, magnetic and electric fields. At this point, the plasma needs to detach itself from the imposed magnetic field to form a free plume. Failure to do so would result in a substantial amount of plasma turning around along the magnetic lines and coming back to the spacecraft, ruining efficiency, attacking sensitive surfaces, and polluting the environment of the payload.

Modeling and simulation of the different processes in these two regions is fundamental for a good understanding of the physics behind the MN, and an essential step towards the design and optimization of a real device. We have recently studied the acceleration region of the MN with the aid of our DIMAGNO code, a two-fluid, two-dimensional code of the partially magnetized, collisionless plasma flow.[8] The influence of ion magnetization and field geometry, the acceleration mechanisms, the formation of longitudinal electric currents and the propulsive performances were investigated. Subsequently, a critical review of detachment theories based on plasma-induced magnetic field, plasma resistivity, and electron inertia was undertaken.[9–12]

At this stage, characterization of the far-region becomes necessary for a proper assessment of the detachment processes in the MN. This article presents a preliminary study of the MN far-field, limited to a low-β, quasineutral, collisionless plasma. To this end, DIMAGNO has been extended to allow the simulation beyond the turning-point of the outermost magnetic streamtube containing plasma, i.e. the MN edge, hence facilitating the study of the plasma far into the downstream region. The paper is structured as follows. Section II briefly highlights the main characteristics of the updated DIMAGNO model. Sections

*PhD student, Equipo de Propulsión Espacial y Plasmas (EP2, web.fmetsia.upm.es/ep2), student AIAA member (mario.merino@upm.es).
†Professor, EP2, senior AIAA member (eduardo.ahedo@upm.es).

Copyright © 2012 by the authors. Published by the American Institute of Aeronautics and Astronautics, Inc., with permission.

III to V pursue the three-fold objectives of this paper: first, we analyze the characteristics and balance of the residual forces in the far-field (section III). Second, we assess the detachment and performances of the produced plasma plume (section IV). Third, we quantify the relevance of secondary effects not included in the model using a perturbation approach (section V), which will provide a valuable indication of the validity of the current model and the necessary extensions for a detailed analysis. Finally, conclusions and concepts requiring further work are gathered in section VI.

II. DIMAGNO model and extension of the code

DIMAGNO's two-fluid model describes the steady-state flow of a fully ionized plasma in a MN. A brief overview of its main aspects is given below. For a detailed description of the model, its equations and the integration procedure, the reader is directed to our previous articles.[8,9,13] The notation followed in this paper is the same as the one therein.

The general equation of motion for a simply-charged species j in a magnetic field B is

$$m_j n_j \left(\boldsymbol{u}_j \cdot \nabla\right) \boldsymbol{u}_j = -\nabla \cdot \mathcal{P} + q_j n_j \left(-\nabla\phi + \boldsymbol{u}_j \times \boldsymbol{B}\right) + \boldsymbol{R}_j, \tag{1}$$

where $\mathcal{P}$ is the pressure tensor, and $\boldsymbol{R}_j = \pm m_e \nu_{ei}(\boldsymbol{u}_i - \boldsymbol{u}_e)$ the corresponding resistive term for each species (minus sign for ions, plus for electrons). Under the hypotheses of (1) quasineutral ($n_i = n_e \equiv n$), collisionless plasma, (2) fully-magnetized, isothermal electrons of negligible inertia, and (3) cold ions, the longitudinal and azimuthal ion equations of motion can be written as

$$m_i \left(\frac{\tilde{u}_i^2}{\rho_i} \mathbf{1}_{\perp i} + \frac{1}{2} \frac{\partial \tilde{u}_i^2}{\partial \mathbf{1}_{\parallel i}} \mathbf{1}_{\parallel i} \right) = -e\nabla\phi + e u_{\theta i} B \mathbf{1}_{\perp}, \tag{2}$$

$$m_i r u_{\theta i} + e\psi = D_i\left(\psi_i\right), \tag{3}$$

whereas the longitudinal electron equation is:

$$0 = -T_e \nabla \ln n + e\nabla\phi - e u_{\theta e} B \mathbf{1}_{\perp}. \tag{4}$$

Note that a collisionless, electron-magnetized flow is a requisite for proper magnetic confinement and thus for an efficiently designed MN thruster. In these expressions, ρ_i and $\tilde{u}_i$ are the meridional curvature radius and velocity of ions, ψ is the magnetic streamfunction, and D_i is a property of the ion streamtube, known from the initial flow conditions. Here, $\mathbf{1}_{\parallel i}$, $\mathbf{1}_{\perp i}$ and $\mathbf{1}_{\parallel}$, $\mathbf{1}_{\perp}$ are meridional unit vectors parallel and perpendicular to ion and magnetic streamtubes, respectively. Full electron magnetization implies $\boldsymbol{u}_e = \tilde{u}_e \mathbf{1}_{\parallel} + u_{\theta e} \mathbf{1}_{\theta}$, and requires dropping the azimuthal electron equation (which can be used to calculate $u_{\perp e}$ as a correction[9,12]). A consequence of this is electron isorotation,[8] i.e., $u_{\theta e}/r = w_{\theta e}\left(\psi\right)$.

Equations (2)–(4) plus the relevant continuity equations (not shown here) constitute a hyperbolic set for the supersonic plasma flow that is integrated from an initial section using the method of characteristics (MoC).[8,14] This approach endows DIMAGNO with high accuracy and speed. The magnetic field is calculated analytically for any distribution of current loops. For moderate plasma-β cases, the plasma-induced magnetic field $\boldsymbol{B}_p$ (which would make the system elliptic) can also be taken into account with a simple iterative process,[11] by taking $\boldsymbol{B} = \boldsymbol{B}_a + \boldsymbol{B}_p$, with $\boldsymbol{B}_a$ the externally-applied field.

DIMAGNO's algorithm has been rewritten to perform the integration in the intrinsic coordinates of the ion trajectories, instead of propagating the characteristic lines in the cylindrical coordinates with z as the parameter. This improvement permits to integrate around and beyond the turning point of the MN, which was previously infeasible when characteristic lines became vertical. Additionally, this upgrade has proven to enhance integration speed and accuracy, which is measured as the error in conservation of total ion momentum and energy.

The resulting model depends on the magnetic field intensity and geometry, and the plasma conditions at the magnetic throat ($z = 0$ and $0 \leq r \leq R$). For the sake of simplicity, the field generated by a simple current loop of radius $R_L = 3.5R$, located at $z = 0$, will conform the MN here. The resulting MN has a mild divergence as depicted in Figure 1, and a turning point located at $(z/R, r/R) \simeq (16, 23)$. The current analysis focuses on MN flows with a simple initial density profile (the one expected to result from a helicon source[15]), low plasma-β (i.e., negligible plasma-induced magnetic field), negligible initial ion rotation , and

Downloaded by Eduardo Ahedo on November 25, 2012 | http://arc.aiaa.org | DOI: 10.2514/6.2012-3843

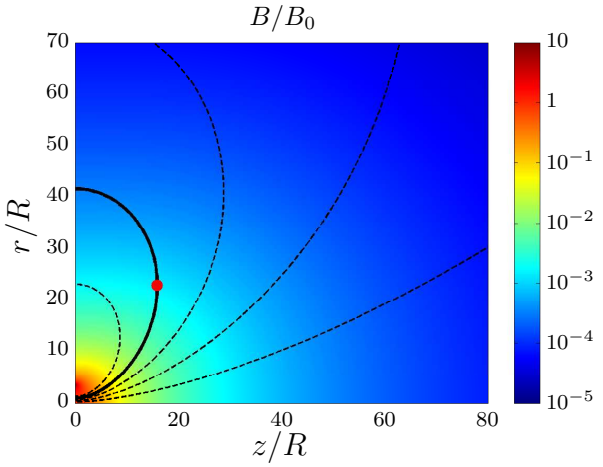

Figure 1. Normalized magnetic field B/B_0 (logarithmic scale) for the single current loop of radius $R_L = 3.5R$. The plasma is injected sonically at the nozzle throat ($z = 0$, $r \leq R$). Selected magnetic lines have been plotted. The thicker line denotes the last plasma streamline in the model. The turning point of the MN has been denoted with a red dot.

Downloaded by Eduardo Ahedo on November 25, 2012 | http://arc.aiaa.org | DOI: 10.2514/6.2012-3843

different degrees of ion magnetization. The flow is then completely defined given the plasma properties at the throat:

$$\begin{aligned} &\tilde{\boldsymbol{u}}_i(r) = \tilde{\boldsymbol{u}}_e(r) = M_0 c_s, && \phi(r) = u_{\theta i}(r) = 0, \\ &n(r) = n_0 J_0(ar/R), && u_{\theta e} = -\left[T_e/(eB)\right] \partial \ln n/\partial r \end{aligned} \tag{5}$$

where we will choose $M_0 = 1.01$ to ensure hyperbolicity in the whole divergent domain, and $a = 0.99a_0$ (where $a_0 = 2.405$ is the first zero of the Bessel function of the first kind J_0). Non-dimensional variables are obtained by normalizing with e, m_i, T_e, n_0 and R, and are denoted with a hat (e.g. $\hat{u}_i = \sqrt{m_i/T_e}u_i$). The intensity of the magnetic field is characterized by the non-dimensional ion gyrofrequency at the origin, $\hat{\Omega}_{i0} = eB(0,0)R/\sqrt{m_i T_e}$. A low magnetization case (simulation 1, with $\hat{\Omega}_{i0} = 0.1$) and a high magnetization case (simulation 2, with $\hat{\Omega}_{i0} = 100$) will be used in the discussions of the following sections. The low ion magnetization case yields in practice the unmagnetized-ion solution. These two simulations cover most of the spectrum of envisaged applications (see tables 1 and 2).

m_i, Kg	10^{-27}–10^{-25} (H–Xe)
B_0, G	200–10000
T_e, eV	5–50
n_0, m^{-3}	10^{16}–10^{20}
R, m	0.01–0.1

Table 1. Typical range of main MN parameters, encompassing the wide spectrum of expected propulsion applications. As an example, the helicon thruster of Ref. 2, operating on Argon or Nitrogen, has $B_0 = 1000$ G, $T_e = 20$ eV, $n_0 = 7 \cdot 10^{18}$ m^{-3}, and $R = 0.01$ m.

$\hat{\Omega}_{i0}$	0.04–500
$\hat{\beta}_0$	10^{-8}–0.1
$\hat{\chi}_0$	10–10^9
$\hat{\ell}_{e0}$	$6 \cdot 10^{-5}$–0.08
$\hat{\lambda}_{D0}$	10^{-5}–10^{-2}

Table 2. Minimal and maximal values of the non-dimensional plasma parameters at the magnetic throat, based on the expected ranges of operation of table 1: ion gyrofrequency $\hat{\Omega}_{i0} = eB_0R/\sqrt{m_i T_e}$; plasma beta $\beta_0 = \mu_0 n_0 T_e/B_0^2$; Hall parameter $\chi_{H0} = \Omega_{e0}/\nu_{ei0}$; electron Larmor radius $\hat{\ell}_{e0} = \sqrt{m_e T_e}/(eB_0 R)$; and Debye length $\hat{\lambda}_{D0} = \sqrt{\varepsilon_0 T_e/(n_0 e^2)}/R$. The large ratio of the parameter m_i/m_e is 1837 for Hydrogen and 239327 for Xenon.

III. Far-field force balance

The far-field plasma expansion is presented in Figure 2, where it is seen that density decreases by several orders of magnitude after the plasma passes the turning point (marked in red in Figure 1). Interestingly, the largest decrease takes place in the peripheral plasma. Both simulations yield very similar results, suggesting that magnetization has little influence in the considered range.

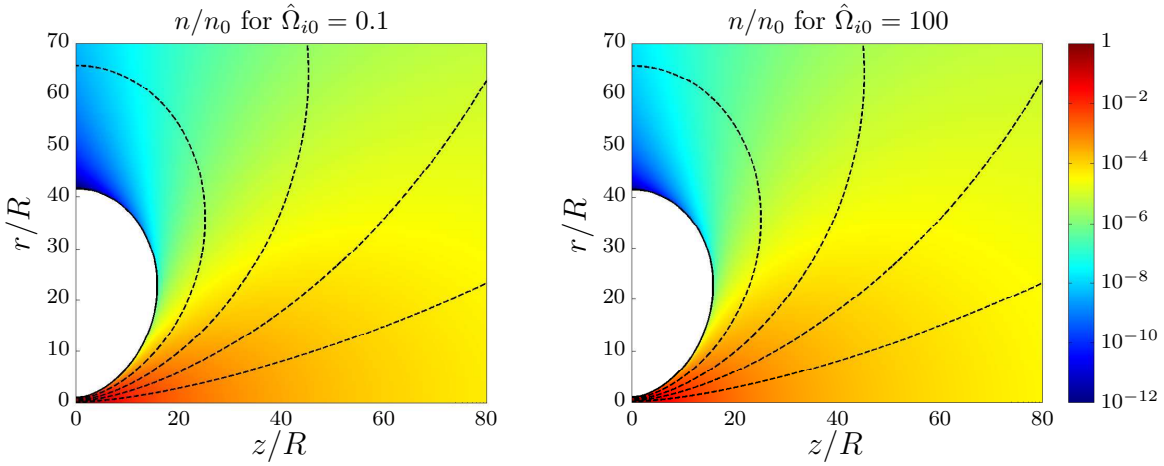

Figure 2. Normalized plasma density n/n_0 (logarithmic scale) in the far-field plume and beyond the turning point of the magnetic field. Magnetic tubes have been indicated in dashed lines. Left: low magnetization; right: high magnetization. Density in the periphery of the plasma is higher in the high-magnetization case.

The forces on the electron fluid control the expansion of the plasma in the MN. According to Eq. (4), a delicate equilibrium forms between the pressure ($-\nabla p_e$), electric ($en\nabla\phi$) and magnetic ($-enu_{\theta e}B\mathbf{1}_\perp$) forces. All three rapidly decrease as the plasma moves into the far region, as can be anticipated by the evolution of density in Figure 2. In spite of this, it is found that the magnitude of these forces per unit particle roughly remains in the same order of magnitude through the far plume, decreasing only at a very low rate. Figure 3 displays the perpendicular pressure gradient per electron, $(\partial p_e/\partial \mathbf{1}_\perp)/\hat{n}$, providing a sense of the magnitude of all other forces-per-particle as well. Throughout the expansion, perpendicular pressure always acts in the outward direction, i.e., $\partial p_e/\partial \mathbf{1}_\perp > 0$, and hence electric and magnetic confinement keeps the plasma away from the thruster (even after the turning point). In the parallel direction, however, pressure is only counteracted by the electrostatic forces. The resulting ambipolar electric field, which couples ion and electron motion, simultaneously accelerates ions. Dashed lines in these plots denote the curves where $\partial p_e/\partial z = 0$ and $\partial p_e/\partial r = 0$. They help identify the regions of the plasma where the plasma pressure acts in the $z > 0$, $r > 0$ direction (region under curve (a)), in the $z < 0$, $r > 0$ direction (region between both curves), and in the $z < 0$, $r < 0$ direction (to the left of curve (b)). Visibly, magnetization degree has only a small influence on them in the range under study.

The competition between electric and magnetic forces to confine the perpendicular pressure defines the character of the expansion. Figure 4 presents the perpendicular magnetic-to-pressure force ratio for the low and high magnetization cases. While initially only $\boldsymbol{B}$ confines the plasma, perpendicular electric fields gradually develop and these gain importance until they eventually dominate the magnetic force. The larger magnetization in simulation 2 results in a larger region of dominance of magnetic forces that extends well into the downstream region. This is a consequence of ions requiring less $E_{\perp i}$ field to expand according to the geometry of the MN, as the perpendicular magnetic force on ions increases the higher $\hat{\Omega}_{i0}$ is (see section IV below). Nevertheless, in all cases electric confinement progressively gains in importance in the far-field. This natural evolution of the force ratio illustrates the smooth transition from a magnetized plasma to a free plume, where the external magnetic interaction must ultimately become negligible.

Regarding the collective behavior of ions and electrons, the model shows that the residual longitudinal magnetic force on the plasma (which is the only external force in the MN), albeit small, is still beneficial. This force continues to confine the plasma locally in the far-field, pushing it away from the thruster even beyond the turning point and hence contributing (minimally) to thrust. Assuming $B_r > 0$ in $(z, r) > 0$

Downloaded by Eduardo Ahedo on November 25, 2012 | http://arc.aiaa.org | DOI: 10.2514/6.2012-3843

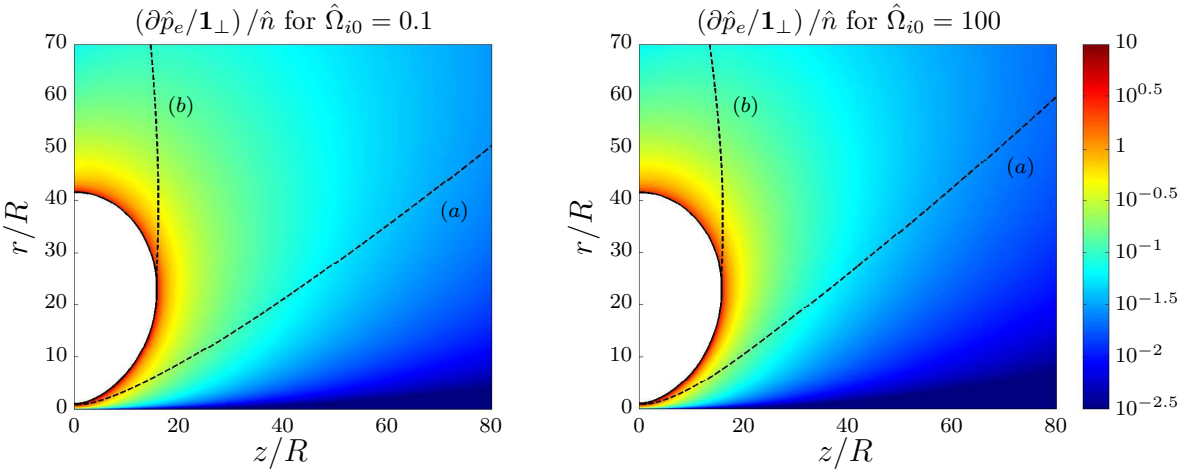

Figure 3. Non-dimensional pressure force per unit particle in the perpendicular direction, $(\partial p_e/\partial \mathbf{1}_\perp)/n$ (logarithmic scale). The lines of $\partial p_e/\partial z = 0$ (a) and $\partial p_e/\partial r = 0$ (b) are also shown in the figure. Left: low magnetization; right: high magnetization.

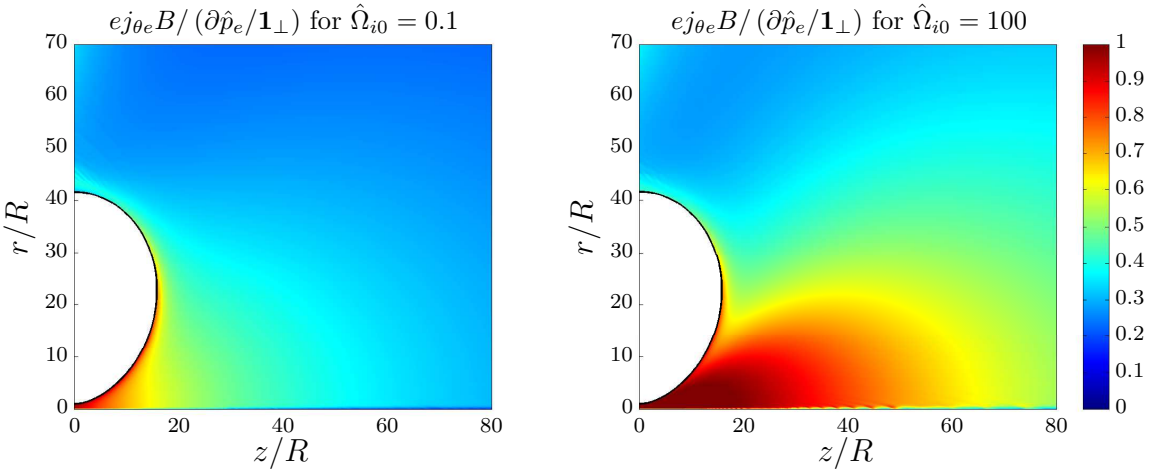

Figure 4. Magnetic-to-pressure force ratio on electrons in the far-field, $ej_{\theta e}B/(\partial p_e/\partial \mathbf{1}_\perp)$. Electric and magnetic perpendicular forces sum up to confine the perpendicular pressure. Left: low magnetization; right: high magnetization.

without loss of generality, the condition for local positive thrust is $u_{\theta i} - u_{\theta e} < 0$, or analogously,

$$\frac{D_i(\psi_i) - e\psi}{m_i r} < r w_{\theta e}(\psi). \tag{6}$$

This is fulfilled in a cylindrical hot plasma in equilibrium (as those expected at the MN throat in propulsive applications), independently of the initial rotation of ions, since the combined magnetic force on ions and electrons needs to confine the existing pressure. Expression (6) helps find regions of the MN, if any, where the magnetic force can reverse, i.e., act to expand and decelerate the plasma. Interestingly, this inversion does not take place in the studied hot plasmas in the region of analysis, not even in the simulation with $\hat{\Omega}_{i0} = 100$ (representative of a practical high-limit case with high $u_{\theta i}$ and low $u_{\theta e}$). In conclusion, the residual magnetic field in the plume should not be regarded as detrimental, for its absence would result in less confinement, and consequently, a more divergent plume. Therefore, the lack of magnetic detachment, in the sense of liberating the plasma from the external magnetic field, constitutes a problem *only* when/where $u_{\theta i} - u_{\theta e} > 0$.

IV. Ion self-detachment and nozzle performance

The motion of ions responds to the geometry of the applied field and the magnetized electron dynamics, as it adapts to fulfill quasineutrality in the plasma domain. When the (small) centrifugal term in $u_{\theta i}^2$ is

Downloaded by Eduardo Ahedo on November 25, 2012 | http://arc.aiaa.org | DOI: 10.2514/6.2012-3843

neglected, Eq. (2) indicates that longitudinal ion trajectory curvature radius ρ_i results from a combination of electric ($eE_{\perp i}$) and magnetic ($eu_{\theta i}B_{\parallel i}$) forces on the ions. A perpendicular electric field develops when ion magnetization is insufficient by itself to deflect the ion trajectories as commanded by the MN. Clearly, the high-magnetization case requires much lower perpendicular fields in order to accomplish the ion expansion (see Figure 4). From Eq. (2), we find that

$$\rho_i \simeq m_i \tilde{u}_i^2 \left(eE_{\perp i} + eu_{\theta i} B_{\parallel i} \right)^{-1}, \tag{7}$$

which highlights the rapid growth of ρ_i in the far-field as u_i increases (see Figure 5), and both the electric and magnetic fields decrease. This expression predicts an eventual transition to almost conical ion streamtubes, which gradually separate from their initial magnetic tubes. This trend is observed in Figure 5, which shows the ion and magnetic streamlines, and ion velocity in the background. It is clear that most of the ion flow *does not turn around with the field*.

Additionally, the perpendicular electric field required for the deflection is associated to a large perpendicular rarefaction, as was seen in Figure 2. This behavior is beneficial, as the bulk of the plasma remains in the core of the plume and hence radial losses are kept small. Only a tiny fraction of the peripheral ions are required to expand beyond the turning point in order to fulfill quasineutrality in this region. This separation of ions from the field can be termed *ion self-detachment*, and facilitates the formation of a free plume.

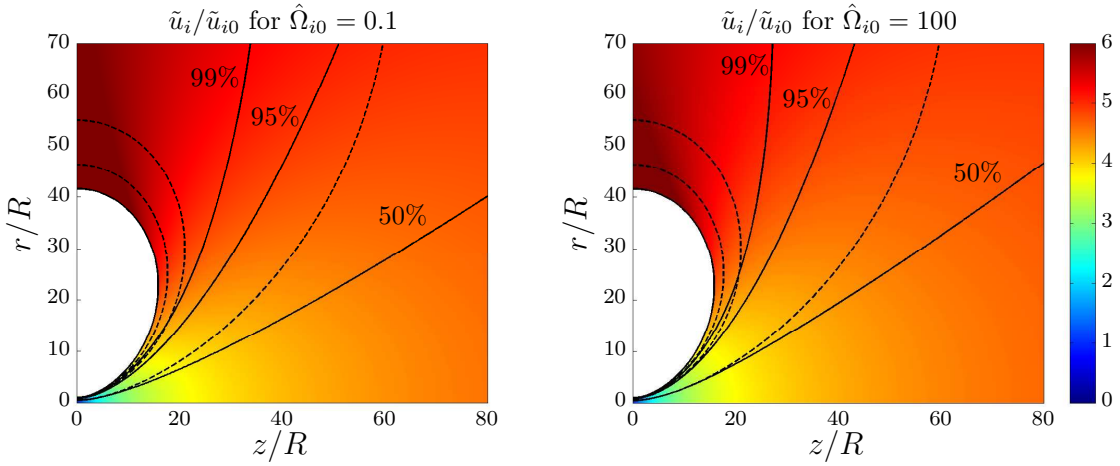

Figure 5. Ion (solid) and magnetic (dashed) streamtubes for both simulations. Each pair of lines initially coincide at the nozzle throat. The tubes of 99% mass flow and initially-coincident magnetic tubes are shown as thicker lines. Normalized ion velocity u_i/u_{i0} (coincident with Mach number M in this isothermal plasmas) is plotted on the background. Left: low magnetization; right: high magnetization.

Magnetization is a key parameter to the final angle of ion trajectories and to the amount of coming-back plasma, as observed in Figure 5. Ions remain attached to the field roughly until $\hat{\Omega}_i \sim 1$. However, the fast decrease of Ω_i ($\Omega_i/\Omega_{i0} = B/B_0$, which is plotted on Figure 1) means that, even for the high magnetization simulation with $\hat{\Omega}_{i0} = 100$, this occurs already before $z/R \simeq 20$. Hence, a much higher $\hat{\Omega}_{i0}$ is needed to keep ions magnetized beyond the turning point ($\hat{\Omega}_{i0} > 10^3$). This explains the slow increase of ion attachment with initial magnetization, and incidentally, also the small differences of n and other variables between each simulation.

It must be noted that the loss of a small fraction of the jet due to back-flowing is not unique to MNs. This phenomenon is common and inherent to any jet propulsion system in vacuum, since a fan-expansion forms at the exit of the thruster to fill the surrounding space and a insignificant amount of propellant expands backwards.[14] The particularity of MNs is that they lack the well-defined "end" that their solid counterparts have, making it difficult to assign them a clear value of the thrust gain and other performance figures, while in solid nozzles these can be evaluated at the exit section. These losses are acceptable when they constitute a negligible fraction of the plume flux. In consequence, a sensible approach to study the propulsive performances of a MN flow is to focus on the bulk of the plume (e.g., the ion tube containing 99% of the ion flux) and neglecting the plasma outside of it. Figure 6 presents thrust and plume efficiency of the plasma contained within the 99% ion mass flow tube, resp. $F_{99\%}$ and $\eta_{plume,99\%}$. These are defined

Downloaded by Eduardo Ahedo on November 25, 2012 | http://arc.aiaa.org | DOI: 10.2514/6.2012-3843

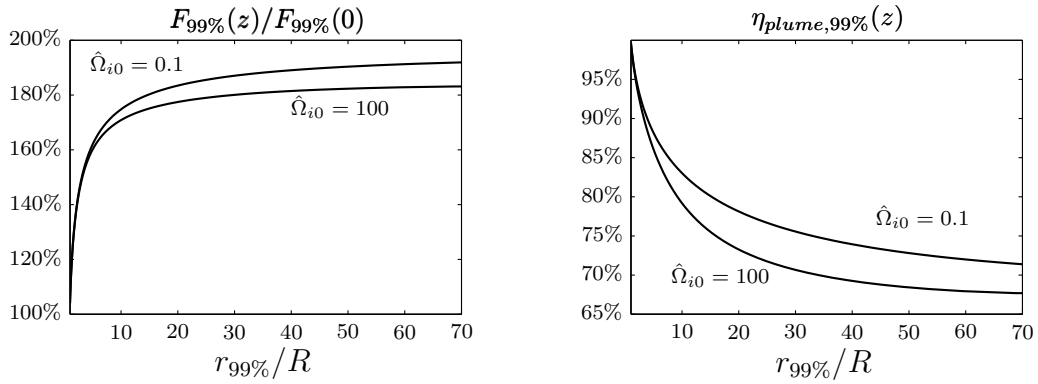

Figure 6. Evolution of thrust and plume efficiency of the plasma contained in the 99% mass flux tube for the low and high magnetization cases. The lines are plotted against $r_{99\%}$, radius of this tube.

as integrals on $z = \text{const}$ sections from the axis to $r = r_{99\%}(z)$, the radius of the 99%-flux tube,

$$F_{99\%}(z) = 2\pi \int_0^{r_{99\%}(z)} nr\left(m_i u_{zi}^2 + T_e\right) dr, \qquad \eta_{plume,99\%}(z) = \frac{\int_0^{r_{99\%}(z)} nr\left(m_i u_{zi}^3\right) dr}{\int_0^{r_{99\%}(z)} nr\left(m_i u_i^2 u_{zi}\right) dr}, \tag{8}$$

and can be calculated at any z (as long as the 99% mass flux line does not turn around). These plots indicate that a higher $\hat{\Omega}_{i0}$ leads to worse MN performances, in agreement with Ref. 8, and also suggest that the rate of variation of these values progressively decreases downstream, where both thrust and efficiency become almost constant (apparently approaching free plume values).

V. Other far-field phenomena and model validity

Apart from the dominant forces described in section III, a number of additional physical effects are present in the plasma, but have been neglected in the model. Although these effects are negligibly small in the near-field of an efficient MN, their role may gain importance or even dominate the expansion in the far-field as the ordering of terms changes in the plasma equations. A careful look is required in order to assess the range of validity of the model, find out which hypotheses are likely to break first, and improve our understanding of how plasma evolves in the plume.

This section aims to explore the significance of the following phenomena in the downstream region: (1) the plasma-induced magnetic field, (2) ion-electron collisions, (3) electron finite Larmor radius (FLR) effects and (4) non-neutral effects. The approach followed here is to analyze the magnitude of these effects as a perturbation to the solution of the ideal model of section II. The forces of all these effects are essentially plasma internal interactions, and as such they can alter the plasma flow but do not directly participate in thrust generation. The interaction between plasma azimuthal currents and the applied field is still the only externally applied force and the only source of thrust in the MN.[8] In addition to the enumerated effects, others such as the presence of ambient particles or background fields could also affect the plume, but these will not be discussed here.

The plasma-induced magnetic field $\boldsymbol{B}_p$ created by the azimuthal currents was studied in Ref. 11 in the near-field of a medium-β plasma. There, it is shown that the relevant parameter for the quantification of B_p/B_a is the local beta $\beta = \mu_0 n/B^2$, which has been plotted in Figure 7 for simulation 1 based on the solution of the ideal model. Notice that the ratio β/β_0 behaves alike in both simulations due to the similar distribution of density n in the far-field. This figure indicates that induced field effects progressively and monotonically become more important in the far-field in the bulk of the plasma, since n decreases slower than B^2 there. This means that, eventually, a region of $\beta = 1$ will occur downstream, and $\boldsymbol{B}_p$ will dominate in the plume thereafter. The induced magnetic field affects mainly the core of the plasma (denser), while leaving the peripheral plasma near the MN edge essentially unaffected. The tendency of B_p (diamagnetic character with respect to B_a) is to expel the field out of the plasma domain. Our preliminary analysis of B_p (Ref. 11) showed that this increases the divergence rate of the nozzle, and can give rise to magnetic separatrices and field-reversed configurations in the plume. A detailed study of these possibilities will be object of future work.

Downloaded by Eduardo Ahedo on November 25, 2012 | http://arc.aiaa.org | DOI: 10.2514/6.2012-3843

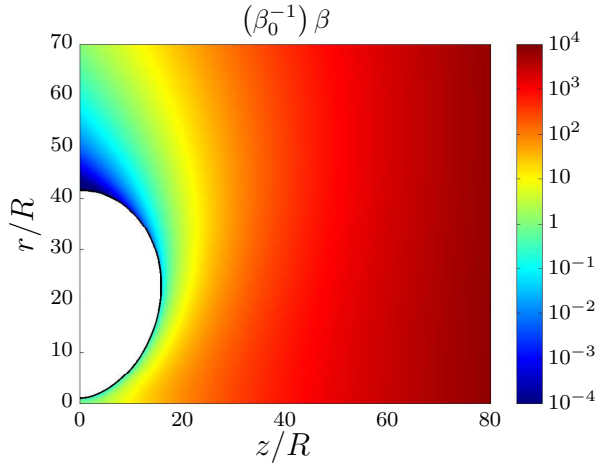

Figure 7. Relative plasma beta β in the MN (logarithmic scale; based on the unperturbed solution), for the $\hat{\Omega}_{i0} = 0.1$ simulation. The normalization with respect to β_0 allows to remove the dependency on the initial conditions. This figure is essentially the same in the $\hat{\Omega}_{i0} = 100$ case, as density behaves similarly in both (see Figure 2). The expected range of values of β_0 can be found in table 2.

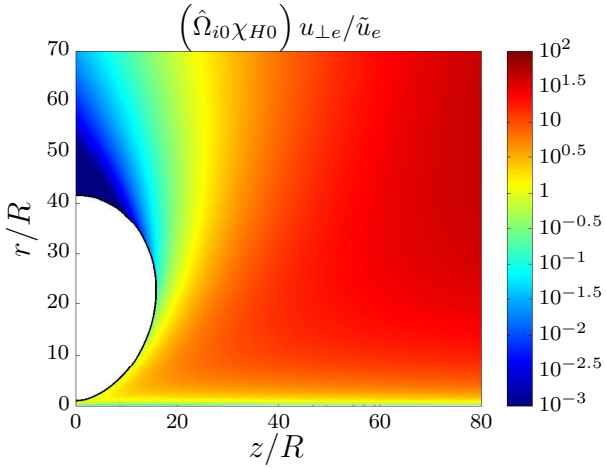

Figure 8. Relative cross-field electron diffusion velocity due to collisions, $u_{\perp e}/u_{\parallel e}$ (as a perturbation to the ideal solution), for the $\hat{\Omega}_{i0} = 0.1$ simulation. The normalization with $\hat{\Omega}_{i0}\chi_{H0}$ helps this figure describe both simulation cases, as χ_H/χ_{H0} (and, consequently, the value plotted here) behaves very similarly in both. χ_{H0} expected range can be found in table 2.

Collisions can facilitate the outwards diffusion of electrons across the B field.[9,10] An adequately high Hall parameter $\chi_H = \Omega_e/\nu_{ei}$, with $\nu_{ei} \propto n/T_e^{3/2}$, ensures negligible plasma resistivity effects, since the cross-field velocity is $u_{\perp e} = u_{\theta e}/\chi_H$ (see Eq. (6) of Ref. 9). The Hall parameter χ_H remains almost constant in the core of the plume and increases several orders of magnitude in the rarefied, peripheral plasma. Note that, due to its dependency on $u_{\theta e}$, the cross-field diffusion $u_{\perp e}$ further decreases for higher $\hat{\Omega}_{i0}$, because the azimuthal velocity satisfies $\hat{u}_{\theta e} \propto 1/\hat{\Omega}_{i0}$. In first approximation, $u_{\perp e}$ can be calculated as a perturbation to the zeroth-order solution. The ratio $u_{\perp e}/\tilde{u}_e$—which measures the local electron- magnetic field separation—is shown in Figure 8. This ratio increases slowly downstream for intermediate radial positions in the plasma, suggesting that electron trajectories can ultimately separate outwards from the magnetic field in the far plume, as $u_{\perp e}$ becomes more important due to collisions. Consequently, this means that resistivity can eventually break the weak residual magnetic confinement in the far plume.

Electron FLR effects (or electron inertia) can also affect the electron trajectories, separating them from the magnetic field. At least one of the multiple FLR effects detaches electrons outwards of the magnetic field,[9,10,12] thus increasing the effective nozzle divergence rate in a similar fashion to collisions. A small ratio of electron Larmor radius ($\ell_e = \sqrt{T_e m_e}/\left(eB\right)$) to electron meridional curvature radius, ℓ_e/ρ_e, indicates proper electron magnetization and inconsequential electron FRL effects.[12] This ratio is displayed in Figure 9, where it can be seen that the largest increase takes place in the periphery of the plume, and well beyond the

Downloaded by Eduardo Ahedo on November 25, 2012 | http://arc.aiaa.org | DOI: 10.2514/6.2012-3843

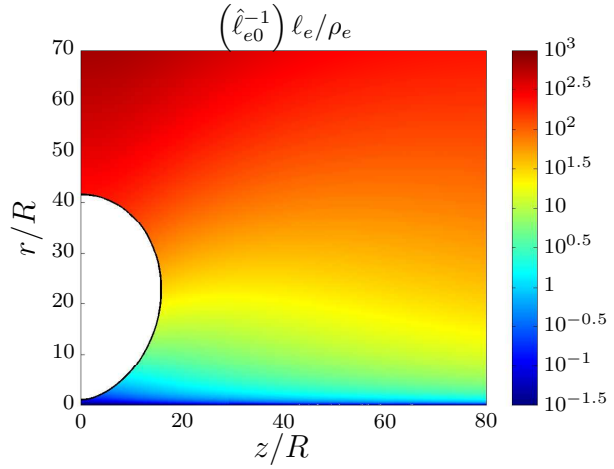

Figure 9. Larmor-to-curvature ratio for electrons, ℓ_e/ρ_e (logarithmic scale). The plot has been normalized with $\hat{\ell}_{e0}$ to remove the dependency on initial plasma conditions and field intensity, making this graph equally valid for both simulation cases. Based on the full electron magnetization solution, $\rho_e \equiv \rho_B$, where $\rho_B = (\boldsymbol{B}/B \cdot \nabla)(\boldsymbol{B}/B)$ is the magnetic curvature radius. Table 2 contains the expected range of values of $\hat{\ell}_{e0}$.

MN turning point. Consequently, initially well-magnetized electrons (i.e., $\hat{\ell}_{e0} \ll 10^{-2}$) remain so in most of the far plume, as electron FLR effects grow very slowly in the downstream direction.

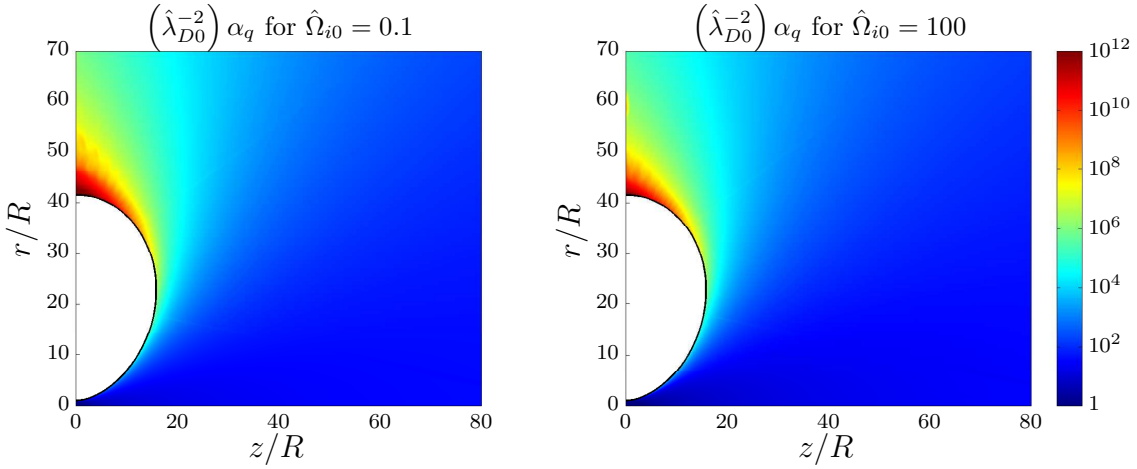

Figure 10. Relative charge density α_q. The factor λ_{D0}^{-2} removes the dependence on initial conditions. Left: low magnetization; right: high magnetization. Table 2 contains the expected range of values of $\hat{\lambda}_{D0}$.

Lastly, the strong rarefaction that takes place in the plume—and specially near the plasma edge—can give rise to non-neutral phenomena, breaking the hypothesis of quasineutrality. Quasineutrality was established to substitute the Poisson equation,

$$\varepsilon_0 \nabla^2 \phi = e\,(n_e - n_i)\,, \tag{9}$$

with $n_i = n_e \equiv n$. The adequacy of this assumption can be checked quantitatively by analyzing the relative charge density $\alpha_q = (n_i - n_e)/n_e$ that results from introducing the potential ϕ of the quasineutral solution into Eq. (9),

$$\alpha_q = -\hat{\lambda}_{D0}^2 \frac{\hat{\nabla}^2 \hat{\phi}}{\hat{n}}, \tag{10}$$

where λ_{D0} is the Debye length of the plasma at the origin. The relative space-charge in the MN is displayed in Figure 10. Clearly, it is negligible in most of the domain for the expected application values of λ_{D0} (see Table 2). However, the large increment near the border of the plasma jet after the turning point suggests that non-neutral effects can be important in this region and that the quasineutrality hypothesis does not hold except for the coldest, densest plasmas (smaller λ_{D0}). Magnetization seems to play a little role on this in the considered range. Non-neutral effects in the periphery of the plasma plume will certainly modify the

Downloaded by Eduardo Ahedo on November 25, 2012 | http://arc.aiaa.org | DOI: 10.2514/6.2012-3843

quasineutral solution, as they set a bound to the increase of the perpendicular electric field, which is the responsible of pushing sideways the ion flow. Therefore, they are expected to further enhance ion detachment from the magnetic field. A detailed study is needed to clarify the consequences of the non-neutral region.

As a final comment to this section, electron cooling (not contemplated in the current model due to the lack of information on the evolution of the electron energy distribution function, and at any rate expected to be small—see for instance Ref. 16) would contribute to reduce the plasma beta β, slightly increase the collision frequency ν_{ei}, and reduce electron Larmor radius ℓ_e. Additionally, the discussed mechanisms can interact with each other. For instance, the induced magnetic field $\boldsymbol{B}_p$ tends to counteract the applied magnetic field $\boldsymbol{B}_a$, thus resulting in a lower effective magnetic field, a lower Hall parameter χ_H, and hence a more important role of collisions.

VI. Conclusions and future work

An analysis of the far-field plasma plume of a magnetic nozzle has been carried out, covering the expected application range of ion magnetization. The balance of residual forces, the gradual detachment of ions, and nozzle performances, have been studied thanks to an improved version of our DIMAGNO code.

Pressure, magnetic and electric forces per particle are all comparable in the far region. Magnetization strength has a large influence on the extent of the region where magnetic forces dominate confinement. As the free-plume forms, the confining electric force gradually gains importance. A criterion was presented to assess whether the applied magnetic field is locally beneficial or detrimental for acceleration and confinement in the plume. This condition was always met in the region under study for all magnetization degrees considered.

Ion and magnetic streamtubes closely coincide until $\hat{\Omega}_i \sim 1$ roughly, after what ion tubes separate and become almost conical as $\tilde{u}_i$ grows. This result highlights that "plasma detachment" does not constitute an issue in the operation of a magnetic nozzle, as the bulk of the plasma naturally separates and forms a free plume. Indeed, only a negligible amount of plasma ($< 1\%$) turns around along the magnetic lines in the studied cases.

Additionally, a preliminary investigation of secondary physical mechanisms in the far plume has been performed using a perturbation approach. The region of validity of each model hypothesis has been discussed based on the throat value of certain parameters. The rapid increase in plasma beta β suggests that induced magnetic field will likely be the first effect to modify the solution in the expected operation regimes. The demagnetization that ensues can enhance other secondary effects such as collisions and electron inertia. Also, we have argued that quasineutrality may not be met at the plasma edge beyond the nozzle turning point.

A more detailed study of these effects must follow to ascertain these results, to better understand their role in the plume formation, and to preclude any negative interaction among them. Other phenomena that have to be carefully examined as well are the influence of ambient plasma and background fields, and the evolution of the electron energy distribution function. Our group is currently developing a hybrid PIC/fluid code named HPMN for the advanced simulation of collisional magnetic nozzle flows,[17] which is proving to be a valuable tool to investigate these aspects.

In summary, all results support the applicability of magnetic nozzles to space propulsion as an efficient mechanism for plasma acceleration and collimated plume formation thanks to the self-detachment of ions. Furthermore, the magnetic field should be kept to a minimum while complying with all other requirements for proper operation, in order to reduce the free-plume divergence angle and to improve overall performance.

Acknowledgments

This work has been sponsored by the Air Force Office of Scientific Research, Air Force Material Command, USAF, under grant number FA8655-12-1-2043. The U.S Government is authorized to reproduce and distribute reprints for Governmental purpose notwithstanding any copyright notation hereon. Additional support for this research was provided by the Gobierno de España (Project AYA-2010-61699).

References

[1]Ziemba, T., Carscadden, J., Slough, J., Prager, J., and Winglee, R., "High Power Helicon Thruster," *41th AIAA/ASME/SAE/ASEE Joint Propulsion Conference & Exhibit*, AIAA 2005-4119, 2005.

[2]Batishchev, O., "Minihelicon Plasma Thruster," *IEEE Transaction on Plasma Science*, Vol. 37, 2009, pp. 1563–1571.

Downloaded by Eduardo Ahedo on November 25, 2012 | http://arc.aiaa.org | DOI: 10.2514/6.2012-3843

[3]Charles, C., Boswell, R., and Lieberman, M., "Xenon ion beam characterization in a helicon double layer thruster," *Applied Physics Letters*, Vol. 89, 2006, pp. 261503.

[4]Pavarin, D., Ferri, F., Manente, M., Curreli, D., Guclu, Y., Melazzi, D., Rondini, D., Suman, S., Carlsson, J., Bramanti, C., Ahedo, E., Lancellotti, V., Katsonis, K., and Markelov, G., "Design of 50W Helicon Plasma Thruster," *31th International Electric Propulsion Conference*, IEPC 2009-205, 2009.

[5]Krülle, G., Auweter-Kurtz, M., and Sasoh, A., "Technology and application aspects of applied field magnetoplasmadynamic propulsion," *J. Propulsion and Power*, Vol. 14, 1998, pp. 754–763.

[6]Tikhonov, V., Semenikhin, S., Brophy, J., and Polk, J., "Performance of 130kw mpd thruster with an external magnetic field and Li as a propellant," *Proceedings of the 25 th International Electric Propulsion Conference*, 1997, pp. 728–733.

[7]Diaz, F., Squire, J., Bengtson, R., Breizman, B., Baity, F., and Carter, M., "The Physics and Engineering of the VASIMR Engine," *36th AIAA/ASME/SAE/ASEE Joint Propulsion Conference & Exhibit*, AIAA 2000-3756, 2000.

[8]Ahedo, E. and Merino, M., "Two-dimensional supersonic plasma acceleration in a magnetic nozzle," *Physics of Plasmas*, Vol. 17, 2010, pp. 073501.

[9]Ahedo, E. and Merino, M., "On plasma detachment in propulsive magnetic nozzles," *Physics of Plasmas*, Vol. 18, 2011, pp. 053504.

[10]Ahedo, E. and Merino, M., "Preliminary assessment of detachment in a plasma thruster magnetic nozzle," 46^{th} *AIAA/ASME/SAE/ASEE Joint Propulsion Conference & Exhibit*, No. AIAA 2010-6613, AIAA, Washington DC, 2010.

[11]Merino, M. and Ahedo, E., "Plasma detachment mechanisms in a magnetic nozzle," 47^{th} *AIAA/ASME/SAE/ASEE Joint Propulsion Conference & Exhibit*, No. AIAA-2011-5999, AIAA, Washington DC, 2011.

[12]Ahedo, E. and Merino, M., "Two-dimensional plasma expansion in a magnetic nozzle: separation due to electron inertia," *Physics of Plasmas*, Vol. 19, 2012, pp. 083501.

[13]Merino, M. and Ahedo, E., "Simulation of plasma flows in divergent magnetic nozzles," *IEEE Transactions on Plasma Science*, Vol. 39, No. 11, 2011, pp. 2938–2939.

[14]Zucrow, M. and Hoffman, J., *Gas dynamics*, Wiley, New York, 1976.

[15]Ahedo, E., "Parametric analysis of a magnetized cylindrical plasma," *Physics of Plasmas*, Vol. 16, 2009, pp. 113503.

[16]Inutake, M., Ando, A., Hattori, K., Tobari, H., and Yagai, T., "Characteristics of a Supersonic Plasma Flow in a Magnetic Nozzle," *J. Plasma Fusion Res.*, Vol. 78, 2002, pp. 1352–1360.

[17]Navarro, J., Merino, M., and Ahedo, E., "Two-Fluid and PIC-Fluid Code Comparison of the Plasma Plume in a Magnetic Nozzle," 48^{th} *AIAA/ASME/SAE/ASEE Joint Propulsion Conference & Exhibit*, No. AIAA-2012-3840, AIAA, Washington DC, 2012.

Downloaded by Eduardo Ahedo on November 25, 2012 | http://arc.aiaa.org | DOI: 10.2514/6.2012-3843